Effects of Triblock Copolymer Architecture and the Degree of Functionalization on the Organoclay Dispersion and Rheology of Nanocomposites

Soobum Choi, Kyung Min Lee, and Chang Dae Han*

Department of Polymer Engineering, The University of Akron, Akron, Ohio 44325

Received December 16, 2003; Revised Manuscript Received June 29, 2004

ABSTRACT: The effects of triblock copolymer architecture (ABA-type vs ABC-type) and the degree of functionalization on the organoclay dispersion in nanocomposites were investigated using X-ray diffraction (XRD), transmission electron microscopy (TEM), and linear dynamic viscoelasticity. For the study, a lamella-forming polystyrene-*block*-polyisoprene-*block*-polystyrene (SIS triblock) copolymer and a homogeneous polyisoprene-*block*-polystyrene-*block*-polybutadiene (ISB triblock) copolymer were synthesized via sequential anionic polymerization. Subsequently, the polyisoprene block of the SIS triblock copolymer was hydroxylated yielding an SIOHS triblock copolymer, and the polybutadiene block of the ISB triblock copolymer was hydroxylated yielding an ISBOH triblock copolymer. The degree of hydroxylation in both SIOHS and ISBOH triblock copolymers was varied. Both the unfunctionalized (SIS and ISB) and functionalized (SIOHS and ISBOH) triblock copolymers were used to prepare nanocomposites with two different types of organoclays: one (Cloisite 30B) treated with a surfactant having hydroxyl groups and the other (Cloisite 15A) treated with a surfactant having *no* hydroxyl groups. It was found from TEM that Cloisite 30B aggregates had a very high degree of dispersion in the ISBOH triblock copolymer, while Cloisite 15A aggregates had a low degree of dispersion in both ISBOH and SIOHS triblock copolymers. A very unusual temperature dependence of linear dynamic viscoelasticity of the ISBOH/Cloisite 30B nanocomposites was observed. An optimum degree of hydroxylation in the ISBOH triblock copolymer existed such that it gave rise to the highest degree of dispersion of Cloisite 30B aggregates. These observations are supported by XRD patterns. In situ Fourier transform infrared spectroscopy confirms the presence of hydrogen bonds in ISBOH/Cloisite 30B nanocomposites and not in ISBOH/Cloisite 15A nanocomposites.

1. Introduction

The nanocomposites composed of layered silicates and a thermoplastic polymer do not provide enhanced mechanical and/or physical properties of the thermoplastic polymer, *unless* the layered silicates and polymer have attractive interactions. When layered silicates and a thermoplastic polymer do not have attractive interactions, there are two ways of addressing the situation: either by modifying the layered silicates with a surfactant such that the surfactant residing at the surface of the layered silicates can have attractive interactions with a specific thermoplastic polymer chosen or by modifying the chemical structure of the polymer so that it can have attractive interactions with the layered silicates. In other words, one must provide chemical affinity between the surface of modified layered silicates (hereafter will be referred to as "organoclay") and a thermoplastic polymer. This has motivated many researchers in both industry and academia to develop surfactants that can be used to chemically modify the surface of layered silicates.

The nanocomposites composed of a thermoplastic polymer and an organoclay have been prepared basically by three different methods: by in situ polymerization, by melt blending, or by solution blending. In conducting in situ polymerization, monomers with functional groups are polymerized in the presence of chemically modified layered silicates, such that the exfoliated layered silicates can be chemically bonded to the polymer matrix. This method was first introduced by the Toyota scientists,[1] and later other research groups[2−5] also prepared organoclay nanocomposites using a similar method. This approach to nanocomposite preparation has an advantage over melt blending or solution blending in that it can give rise to a very high degree of exfoliation of layered silicate aggregates in the nanocomposites. This is because the viscosity of monomers is so low that they can easily approach the layered silicate aggregates to separate the top and bottom layers as promoted by the application of shear stress. However, in situ polymerization of monomers in the presence of chemically modified layered silicates is not always possible, and thus under such circumstances melt blending or solution blending must be employed to prepare organoclay nanocomposites.

When a thermoplastic polymer is mixed with an organoclay, it either intercalates or exfoliates the layered silicate aggregates. In general, intercalation is observed when a polymer matrix and layered silicates do not have sufficient attractive interactions, while exfoliation is observed when a polymer matrix and layered silicates have strong attractive interactions. From the point of view of obtaining markedly improved physical/mechanical properties of nanocomposites, exfoliation is preferred to intercalation. Thermodynamic aspects of intercalation and exfoliation of layered silicates in the preparation of nanocomposites have been investigated.[6−9]

During the past decade many research groups reported on the preparation and characterization of layered silicate nanocomposites based on thermoplastic polymers. There are too many papers (hundreds) to cite them all here. The interested readers are referred to our recent papers[10,11] that cited some representative publications on the subject.

10.1021/ma030585s CCC: $27.50
Published on Web 08/28/2004

Elastomeric block copolymers offer some unique properties in that they contain microdomain structures (spheres, cylinders, gyroids, or lamellae) providing the properties of cross-linked materials and yet retaining elastomeric properties at service temperatures. There are several different types of block copolymers: AB-type diblock, ABA-type triblock, ABC-type triblock, and A_nB_n-type radial block. Such elastomeric block copolymers have long been used in many important industrial applications. There are too many references for the synthesis and characteristics of block copolymers to cite them all here. The readers are referred to some selected monographs that describe unique physical/mechanical properties of elastomeric block copolymers.[12−14] In almost all cases, elastomeric block copolymers are obtained by sequential anionic polymerization that imposes very stringent requirements on the purity of monomers and initiator. It is a well-established fact that the "living" anionic polymerization stops in the presence of even very minute amounts of impurities and/or foreign substances. For this reason, it is *not* possible to prepare end-tethered layered silicate nanocomposites based on block copolymers using in situ anionic polymerization of monomers in the presence of chemically modified layered silicates. Thus, one must employ melt blending or solution blending to prepare layered silicate nanocomposites based on block copolymers.

To date, a relatively small number of studies[15−20] have been reported on the preparation, characterization, and/or rheology of organoclay nanocomposites based on elastomeric block copolymers. The majority of the studies[15−19] employed *unfuntionalized* block copolymers to prepare organoclay nanocomposites and observed only intercalation of organoclay aggregates. Such observations are not surprising, because there were no attractive interactions between the organoclay and the block copolymer matrix employed. In a recent study,[20] Lee and Han investigated the dispersion characteristics of organoclay aggregates in nanocomposites composed of a polystyrene-*block*-hydroxylated polyisoprene (SIOH diblock) copolymer and a commercial organoclay that had been treated with a surfactant having hydroxyl groups. They observed, via transmission electron microscopy (TEM), a high degree of dispersion (exfoliation) of organoclay aggregates in the SIOH diblock copolymer matrix but a low degree of dispersion of organoclay aggregates in *unfunctionalized* polystyrene-*block*-polyisoprene (SI diblock) copolymer matrix. They explained the observed differences in the dispersion characteristics of organoclay aggregates between the two nanocomposites, by showing via Fourier transform infrared spectroscopy that hydrogen bonds were formed between the hydroxyl groups in a surfactant residing at the surface of the organoclay and the hydroxyl groups in the SIOH diblock copolymer matrix, while no hydrogen bonds were formed between the organoclay and SI diblock copolymer matrix. Thus, they concluded that attractive interactions between the organoclay and functionalized SIOH block copolymer played a key role in achieving a very high degree of exfoliation of organoclay aggregates in the nanocomposites.

In the present study, we prepared organoclay nanocomposites based on two different types of block copolymer, ABA- and ABC-types, and then characterized them using X-ray diffraction, TEM, and linear dynamic viscoelasticity. For the study, we employed two organoclays, one treated with a surfactant having hydroxyl groups and the other treated with a surfactant having *no* hydroxyl groups. The primary purpose of the present study was to investigate the effects of triblock copolymer architecture (ABA-type vs ABC-type) with or without functional groups and the degree of functionalization of the respective triblock copolymers on the dispersion characteristics of organoclay aggregates and the linear dynamic viscoelasticity of triblock copolymer/organoclay nanocomposites. In this paper, we report the highlights of our findings.

2. Experimental Section

2.1. Materials and Preparation of Nanocomposites. (a) Synthesis of SIS Triblock Copolymer. We synthesized, via sequential anionic polymerization, an SIS triblock copolymer having approximately an equal block composition. Three steps are required to synthesize an SIS triblock copolymer: (i) purification of a precursor for difunctional initiator, (ii) preparation of difunctional initiator, and (iii) sequential anionic polymerization of styrene and isoprene monomers. First, we purified a precursor, 1,3-bis(phenylethenyl)benzene (PEB) (yellowish liquid) received from Dow Chemical Company, using the chromatographic column packed with activated silica gel with sizes of 230−400 mesh (Selecto Scientific). Next, dilithium initiator (DLI) was prepared by reacting 2 mol of *sec*-butyllithium (BuLi) with 1 mol of PEB in cyclohexane.

For the anionic polymerization of isoprene and styrene monomers sequentially, the following procedures were used. First, cyclohexane and isoprene were vacuum distilled, and pentamethyldiethylenetriamine (PMDETA) (Aldrich) needed to obtain narrow molecular weight polyisoprene was purified by vacuum distillation in the presence of calcium hydride. A mixture of PMDETA and *sec*-BuLi (0.18/1: v/v) was added to the reactor using a syringe. The reactor was then purged with argon gas and heated, while stirring, to 55 °C using a water bath. When the temperature of the water bath reached about 55 °C, DLI was added to first polymerize the isoprene monomer. About 2 h after the addition of DLI, styrene monomer was added to the reactor. After the copolymerization of isoprene and styrene monomers for 1.5 h, a small amount of degassed methanol was added to terminate the living polymers, at which point the color of the solution changed from yellowish red to colorless. Then the reactor temperature was lowered to room temperature, and the solution was precipitated by addition of an excess amount of methanol. The precipitated polymer was filtered and dried at room temperature for 3 days in a fume hood and then at 60 °C for 12 h in a vacuum oven.

(b) Synthesis of ISB Triblock Copolymer. Anionic polymerization with the sequence of isoprene (I), styrene (S), and butadiene (B) was conducted to synthesize an ISB triblock copolymer having high 1,4-addition in PI block, and high 1,2-addition in PB block. For the polymerization, isoprene monomer was first polymerized followed by styrene monomer using cyclohexane as solvent and *sec*-BuLi as initiator, and butadiene monomer was polymerized in the presence of a polar additive, 1,2-dipiperidinoethane (DIPIP).[21] After isoprene monomer was polymerized for 2 h, the purified styrene monomer was added to the reactor at 55 °C using a gastight syringe. Upon the addition of the styrene monomer, the color of the solution changed immediately to orange. The polymerization of styrene monomer was allowed to continue for 1 h and then cooled to 20 °C in an ice−water bath. Subsequently, DIPIP with a molar ratio of 1.0 mol of DIPIP/1.0 mol of *sec*-BuLi was added to the reactor at 20 °C using a gastight syringe and evacuated. After thorough stirring, the purified-liquid butadiene monomer was transferred into the reactor using a double-ended needle from the purified butadiene liquid storage cylinder with known weight, which was then filled with argon gas at a slightly positive pressure at 15 °C. Upon the addition of butadiene monomer, the color changed from orange to yellow and then finally to colorless. After polymerizing butadiene monomer for 12 h, the reaction was terminated by adding 2 mL of degassed methanol using a gastight syringe, at which point the viscosity

Table 1. Molecular Characteristics of the SIS, SIOHS, ISB and ISBOH Triblock Copolymers Synthesized in This Study

sample code	M_n[a]	M_w/M_n[a]	w_{PS}[b]	w_{PI}[b]	w_{PB}[b]	deg of hydroxylation (mol %)[b]
ISB	9.6×10^3	1.15	0.34	0.36	0.30	0
ISBOH-16	9.7×10^3	1.14				16
ISBOH-24	9.6×10^3	1.15				24
ISBOH-39	9.6×10^3	1.15				39
SIS	3.7×10^4	1.10	0.46	0.54		0
SIOHS-16	3.9×10^4	1.09				16
SIOHS-32	3.7×10^4	1.11				32

[a] Determined from GPC against polystyrene standards. [b] Weight fraction determined from ^{1}H NMR spectroscopy.

of the solution dropped suddenly. The polymer was precipitated by the addition of an excess amount of methanol. The precipitated polymer was filtered and dried for 3 days at room temperature in a fume hood and finally dried in a vacuum oven.

(c) Characterization of the Polymers Synthesized. Gel permeation chromatography (GPC) (Waters) was used to determine the number-average molecular weight (M_n) and the polydispersity index (M_w/M_n) of each block copolymer synthesized. Block copolymer composition was determined using ^{1}H NMR spectroscopy. Table 1 gives a summary of sample codes and the number-average molecular weight (M_n) and the molecular weight distribution (M_w/M_n), determined by gel permeation chromatography (GPC) against polystyrene standards, of the SIS and ISB triblock copolymers synthesized in this study. The PI block of the SIS triblock copolymer has the following microstructures: 42.7% 3,4-addition, 24.6% 1,2-addition, and 32.7% 1,4-addition. The PB block of the ISB triblock copolymer has the following microstructures: 68.9% 1,2-addition, 17.7% 1,4-addition, and 13.4% cyclopentane units formed by the addition of polar additive DIPIP. The PI block of the ISB triblock copolymer has the following microstructures: 95.4% 1,4-addition and 4.6% 3,4-addition. The microstructures were determined using ^{1}H NMR spectroscopy.

(d) Hydroxylation of SIS and ISB Triblock Copolymers. The PI block in the SIS triblock copolymer was hydroxylated to obtain SIOHS triblock copolymer, and the PB block in the ISB triblock copolymer was selectively hydroxylated to obtain ISBOH triblock copolymer using hydroboration/oxidation reactions.[22,23] To investigate the effect of the amounts of hydroxyl group in ISBOH or SIOHS triblock copolymers on the dispersion characteristics of organoclay aggregates, we varied the degree of hydroxylation of 1,2-addition of PB block in the ISB triblock copolymer and the degree of hydroxylation of PI block in the SIS triblock copolymer. Table 1 gives a summary of sample codes and the values of M_n and M_w/M_n for the ISBOH and SIOHS triblock copolymers prepared in this study, in which the number next to ISBOH or SIOHS denotes the mol % of hydroxyl group. The GPC traces of the ISBOH and SIOHS triblock copolymers prepared are given in the Supporting Information. The details of the hydroboration/oxidation reactions employed are described in our previous paper.[24] It has been reported[23] that the reactivity of 1,2- and 3,4-additions in PI or PB blocks to hydroboration/oxidation reactions is much greater than that of 1,4-addition. Figure 1 shows ^{1}H NMR spectra for (a) ISB triblock copolymer and (b) ISBOH triblock copolymer. Comparison of Figure 1b with Figure 1a indicates that after hydroboration/oxidation reactions of the ISB triblock copolymer, all of the 1,2-addition in the PB block has been hydroxylated, leaving only 1,4-addition in the remaining PB block of the resultant ISBOH triblock copolymer, and little or no amount of 1,4-addition in the PI block of the ISB triblock copolymer was hydroxylated. That is, a selective hydroxylation of PB block alone in the IBS triblock copolymer occurred.

(e) Preparation of Nanocomposites. To prepare nanocomposites with a functionalized SIOHS (or ISBOH) triblock copolymer, we employed two commercial organoclays (Southern Clay Products): (i) Cloisite 30B treated with a surfactant (MT2EtOH) having the chemical structure methyl, tallow, bis-2-hydroxyethyl, quaternary ammonium chloride[25]

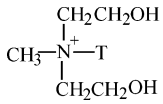

MT2EtOH

where N^+ denotes quaternary ammonium chloride and T denotes tallow consisting of ca. 65% C18, ca. 30% C16, and ca. 5% C14; (ii) Cloisite 15A treated with a surfactant (2 M2HT) having the chemical structure methyl, hydrogenated tallow, quaternary ammonium chloride[25]

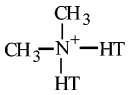

2M2HT

where N^+ denotes quaternary ammonium chloride and HT denotes hydrogenated tallow consisting of ca. 65% C18, ca. 30% C16, and ca. 5% C14. It should be mentioned that 100% of Na^+ ions in natural montmorillonite have been exchanged. The rationale behind the choice of the two organoclays lies in that Cloisite 30B has hydroxyl groups, while Cloisite 15A does not, as confirmed by Fourier transform infrared (FTIR) spectroscopy.[11] Therefore, we were able to investigate (i) the effect of hydroxyl groups in Cloisite 30B when it is mixed with SIOHS and ISBOH, and (ii) the effect of the difference in gallery distance between Cloisite 15A and Cloisite 30B when each is mixed with any of the triblock copolymer synthesized in this study. We prepared several different nanocomposites by solution blending; namely, a predetermined amount of block copolymer was dissolved in a cosolvent of THF/H_2O (90:10 v:v), and then an organoclay in a cosolvent of THF/H_2O was added slowly, while stirring, into the block copolymer solution. This mixture was evaporated slowly under constant stirring for 2 days. After the mixture of a block copolymer and organoclay was dried completely in a vacuum oven at temperatures well above the boiling point of the solvent and also at ca. 20 °C above the glass transition temperature (T_g) of the block copolymer until no weight changes were detected. Table 2 gives a summary of sample codes of the nanocomposites prepared. The amount of organoclay used was 5 wt % in all nanocom-

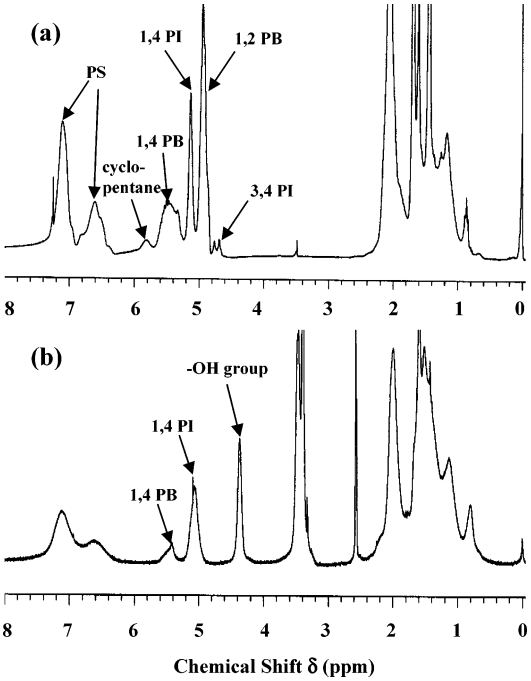

Figure 1. ^{1}H NMR spectra for triblock copolymers (a) ISB and (b) ISBOH.

Table 2. Sample Codes of the Nanocomposites Investigated in This Study[a]

sample code	degree of hydroxylation
(a) SIS and SIOHS Nanocomposites	
SIS/Cloisite 15A	neat SIS triblock copolymer
SIS/Cloisite 30B	neat SIS triblock copolymer
(SIOHS-16)/Cloisite 15A	16 mol % hydroxyl group in the SIOHS triblock copolymer
(SIOHS-32)/Cloisite 15A	32 mol % hydroxyl group in the SIOHS triblock copolymer
(SIOHS-16)/Cloisite 30B	16 mol % hydroxyl group in the SIOHS triblock copolymer
(SIOHS-32)/Cloisite 30B	32 mol % hydroxyl group in the SIOHS triblock copolymer
(b) ISB and ISBOH Nanocomposites	
ISB/Cloisite 15A	neat ISB triblock copolymer
ISB/Cloisite 30B	neat ISB triblock copolymer
(ISBOH-16)/Cloisite 15A	16 mol % hydroxyl group in the ISBOH triblock copolymer
(ISBOH-16)/Cloisite 30B	16 mol % hydroxyl group in the ISBOH triblock copolymer
(ISBOH-24)/Cloisite 15A	24 mol % hydroxyl group in the ISBOH triblock copolymer
(ISBOH-24)/Cloisite 30B	24 mol % hydroxyl group in the ISBOH triblock copolymer
(ISBOH-39)/Cloisite 15A	39 mol % hydroxyl group in the ISBOH triblock copolymer
(ISBOH-39)/Cloisite 30B	39 mol % hydroxyl group in the ISBOH triblock copolymer

[a] All nanocomposites have 5 wt % organoclay.

posites. Since the amount of surfactant MT2EtOH on the surface of Cloisite 30B is 32 wt %, the net amounts of clay are 3.4 wt % clay in each nanocomposite.

According to the Technical Properties Bulletin[25] from Southern Clay Products, the amount of surfactant MT2EtOH residing at the surface of Cloisite 30B is 90 mequiv/100 g and the amount of surfactant 2M2HT residing at the surface of Cloisite 15A is 125 mequiv/100 g. We have been informed from Southern Clay Products that an extremely small amount of excess surfactant is present at the surface of Cloisite 30B, while about 30% excess surfactant is present at the surface of Cloisite 15A. In the present study we used Fourier transform infrared resonance (FTIR) spectroscopy on Cloisite 30B (i) as received from Southern Clay Products and (ii) after being washed with methanol. The FTIR spectra obtained are given in Supporting Information. We have found that the FTIR spectra for the two samples are virtually identical, indicating that little, if any, excess amount of surfactant is present at the surface of Cloisite 30B. Since there is no hydroxyl group in the surfactant 2M2HT residing at the surface of Cloisite 15A, we could not determine, via FTIR spectroscopy, any excess amount of surfactant residing at the surface of Cloisite 15A. On the other hand, we have been informed by Southern Clay Products that after washing with methanol, the amount of surfactant 2M2HT remaining at the surface of Cloisite 15A will be 95 mequiv/100 g, which then becomes identical to organoclay Cloisite 20A. In the present study we prepared nanocomposites with or without washing the organoclays, Cloisite 30B and Cloisite 15A.

2.2. X-ray Diffraction (XRD). Using a Rigaku X-ray generator operated at 40 kV and 40 mA, X-ray diffraction patterns were obtained to determine the mean interlayer spacing of the (001) plane (d001) for the clay (Cloisite 15A or Cloisite 30B) and its nanocomposites with a block copolymer. The X-ray beam was monochromatized to Cu Kα with a graphite crystal. The range of 2θ scanning of X-ray intensity employed was 1.5−10 deg.

2.3 Transmission Electron Microscopy (TEM). TEM images of specimens were taken at room temperature. The ultrathin sectioning (50−70 nm) was performed via cryoultramicrotomy at −80 °C for all block copolymers and at room temperature for all nanocomposites prepared using a Reichert Ultracut E low-temperature sectioning system. A transmission electron microscope (JEM1200EX 11, JEOL) operated at 120 kV was used to obtain images of the neat block copolymer or nanocomposite specimens.

2.4 Fourier Transform Infrared Spectroscopy (FTIR). Using a Fourier Transform Infrared spectrometer (16 PC FTIR, Perkin-Elmer), in situ FTIR spectra were obtained at various temperatures ranging from 30 to 200 °C for all nanocomposites prepared. Spectral resolution was maintained at 4 cm^{-1}. The temperature was measured at the sample surface and controlled to within ±1.0 °C using a proportional-integral-derivative controller. Specimens were maintained at a preset temperature for 5 min prior to data acquisition. Dry argon gas was used to purge the sample compartment to reduce the interference of water and carbon dioxide in the spectrum. Thin films suitable for FTIR were prepared by casting 2% (w/v) solution in THF directly on the KBr salt plate. Film thickness was adjusted such that the maximum absorbance of any band was less than 1.0, at which the Beer−Lambert law is valid. Each film was slowly dried for 24 h in a fume hood until most of the solvent evaporated and then dried at 70 °C for a few days in a vacuum oven. Samples were then stored in a vacuum oven until use.

2.5 Rheological Measurements. An Advanced Rheometric Expansion System (ARES, TA Instrument) was used to conduct, using a parallel-plate fixture, isochronal dynamic temperature sweep experiments of block copolymer/organoclay nanocomposites, measuring the dynamic storage modulus (G') at an angular frequency of 0.1 rad/s during heating, where temperature was increased stepwise in 2 °C/min increments. We also conducted dynamic frequency sweep experiments using a parallel-plate fixture, measuring the storage and loss moduli (G' and G'') as functions of angular frequency (ω) (ranging from 0.01 to 100 rad/s) at various temperatures, for which a fixed strain of 0.04 was used to ensure that measurements were taken well within the linear viscoelastic range of the materials investigated. Further, we investigated intermittent shear flow of the triblock copolymer/organoclay nanocomposites after a rest upon cessation of the initial transient shear flow using a cone-and-plate fixture. For this, we varied the period of rest upon cessation of the initial transient. The temperature control was accurate to within ±1 °C. All rheological experiments were conducted under a nitrogen atmosphere to avoid oxidative degradation of the samples.

3. Results and Discussion

3.1. Dispersion Characteristics of the Nanocomposites Based on SIS and SIOHS Triblock Copolymers. Figure 2 gives XRD patterns (i) for Cloisite 15A and its nanocomposites with SIS and SIOHS triblock copolymers with two different degrees of hydroxylation (16 and 32 mol %) and (ii) for Cloisite 30B and its nanocomposites with SIS and SIOHS triblock copolymers with two different degrees of hydroxylation (16 and 32 mol %). The following observations are worth noting in Figure 2. The d spacing (3.1 nm) of Cloisite 15A is larger than the d spacing (1.9 nm) of Cloisite 30B. The d spacing of Cloisite 15A is increased from 3.1 to 4.0 nm in the SIS/Cloisite 15A and SIOHS/Cloisite 15A nanocomposites, independent of the chemical structure of the block copolymers (SIS vs SIOHS triblock copolymers), and also independent of the degree of hydroxylation (16 vs 32 mol %) in SIOHS triblock copolymer.

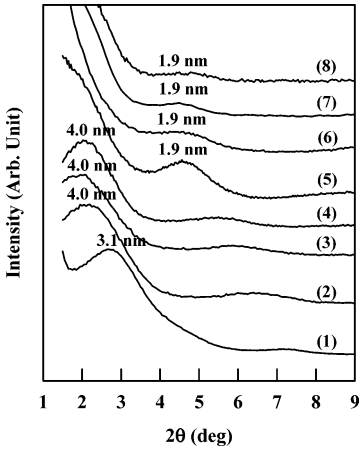

Figure 2. XRD patterns: (1) Cloisite 15A; (2) SIS/Cloisite 15A nanocomposite; (3) (SIOHS-16)/Cloisite 15A nanocomposite; (4) (SIOHS-32)/Cloisite 15A nanocomposite; (5) Cloisite 30B; (6) SIS/Cloisite 30B nanocomposite; (7) (SIOHS-16)/Cloisite 30B nanocomposite; (8) (SIOHS-32)/Cloisite 30B nanocomposite.

We do not think that a slight increase (0.9 nm) in the *d* spacing of Cloisite 15A after being mixed with the SIS or SIOHS triblock copolymers is significant, suggesting that Cloisite 15A has very weak attractive interactions with the SIS and SIOHS triblock copolymers. The *d* spacing of Cloisite 30B remains the same before and after it is mixed with the SIS or SIOHS triblock copolymers, indicating that Cloisite 30B also has little or no attractive interactions with the SIS and SIOHS triblock copolymers. The very small difference in the *d* spacing between Cloisite 15A and the SIS/Cloisite 15A, (SIOHS-16)/Cloisite 15A, or (SIOHS-32)/Cloisite 15A nanocomposites, observed in Figure 2, can be understood from the point of view that there would be little or no attractive interactions (compatibility) between the surfactant 2M2HT residing at the surface of Cloisite 15A and SIS or SIOHS triblock copolymers. Likewise, we can understand the reason no difference in the *d* spacing between Cloisite 30B and the SIS/Cloisite 30B nanocomposite is observed in Figure 2 because there is little or no compatibility between the surfactant MT2EtOH residing at the surface of Cloisite 30B and the SIS triblock copolymer. However, it seems somewhat strange (or it is unexpected at first glance) to learn from Figure 2 that we observe no difference in *d* spacing between Cloisite 30B and the (SIOHS-16)/Cloisite 30B or (SIOHS-32)/Cloisite 30B nanocomposites, although the hydroxyl groups in the surfactant MT2EtOH residing at the surface of Cloisite 30B and the hydroxyl groups in the SIOHS triblock copolymer could potentially have attractive interactions via hydrogen bonding which, however, apparently did not take place.

Figure 3 gives TEM images for (SIOHS-16)/Cloisite 15A and (SIOHS-16)/Cloisite 30B nanocomposites, in which we observe a very low degree of dispersion of both Cloisite 15A and Cloisite 30B in the respective nanocomposites. This observation is consistent with that made above from the XRD patterns given in Figure 2. In other words, in the absence of attractive interactions between the organoclay (Cloisite 15A or Cloisite 30B) and polymer matrix (SIS or SIOHS triblock copolymers) a high degree of dispersion of organoclay aggregates would not occur.

3.2. Dispersion Characteristics of the Nanocomposites Based on ISB and ISBOH Triblock Copolymers. Figure 4 gives XRD patterns (i) for Cloisite 15A and its nanocomposites with ISB and ISBOH triblock copolymers with three different degrees of hydroxylation (16, 24, and 39 mol %) and (ii) for Cloisite 30B and its nanocomposites with ISB and ISBOH triblock copolymers with three different degrees of hydroxylation (16, 24, and 39 mol %). It is seen in Figure 4 that the *d* spacing of Cloisite 15A in the ISB/Cloisite 15A and ISBOH/Cloisite 15A nanocomposites is very close to that in the SIS/Cloisite 15A and SIOHS/Cloisite 15A nano-

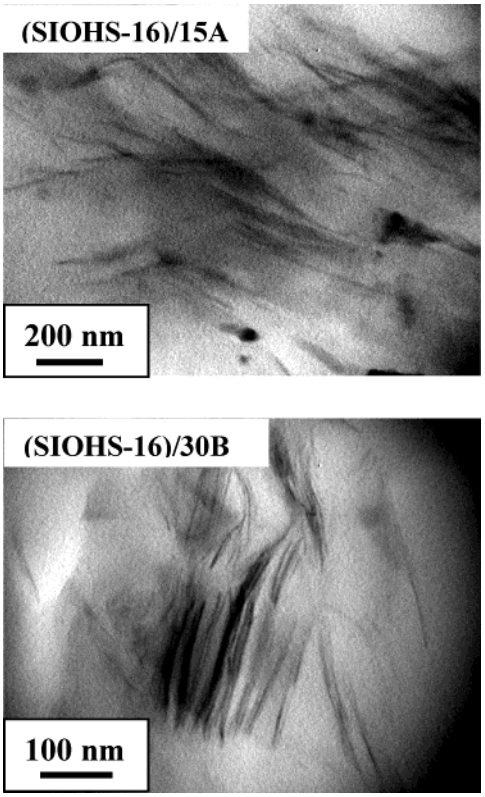

Figure 3. TEM images of (SIOHS-16)/Cloisite 15A nanocomposite and (SIOHS-16)/Cloisite 30B nanocomposite, in which the dark areas represent the clay and the gray/white areas represent the polymer matrix.

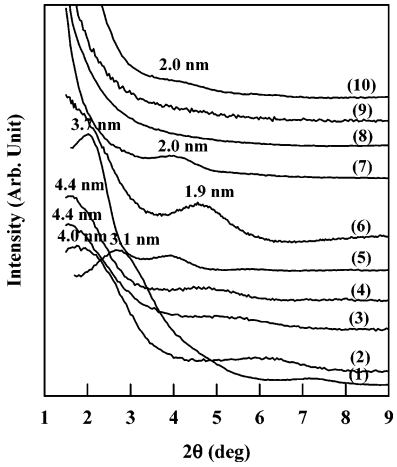

Figure 4. XRD patterns: (1) Cloisite 15A; (2) ISB/Cloisite 15A nanocomposite; (3) (ISBOH-16)/Cloisite 15A nanocomposite; (4) (ISBOH-24)/Cloisite 15A nanocomposite; (5) (ISBOH-39)/Cloisite 15A nanocomposite; (6) Cloisite 30B; (7) ISB/Cloisite 30B nanocomposite; (8) (ISBOH-16)/Cloisite 30B nanocomposite; (9) (ISBOH-24)/Cloisite 30B nanocomposite; (10) (ISBOH-39)/Cloisite 30B nanocomposite.

composites (compare Figure 4 with Figure 2). This observation can be understood from the point of view that there are little or no attractive interactions between the surfactant 2M2HT residing at the surface of Cloisite 15A and ISB or ISBOH triblock copolymers. Notice in Figure 4 that the *d* spacing of ISB/Cloisite 30B nanocomposite is virtually the same as that of Cloisite 30B. Again, this experimental observation can be explained by the expectation that the surfactant MT2EtOH residing at the surface of Cloisite 30B and ISB triblock copolymers are not compatible.

However, in Figure 4 we observe quite different and very interesting XRD patterns in some of the ISBOH/Cloisite 30B nanocomposites. Specifically, we cannot discern an intensity peak from the XRD patterns for the (ISBOH-16)/Cloisite 30B and (ISBOH-24)/Cloisite 30B nanocomposites, while a very weak intensity peak from the XRD patterns is discernible for the (ISBOH-39)/Cloisite 30B nanocomposite giving rise to a *d* spacing of ca. 2.0 nm for the Cloisite 30B in the nanocomposite. The very broad, indistinguishable intensity peak from the XRD patterns for both the (ISBOH-16)/Cloisite 30B and (ISBOH-24)/Cloisite 30B nanocomposites suggests to us that Cloisite 30B aggregates might have been very well dispersed in ISBOH-16 and ISBOH-24. Note that the (ISBOH-39)/Cloisite 30B nanocomposite has ISBOH-39 with 39 mol % hydroxyl group, the (ISBOH-16)/Cloisite 30B nanocomposite has ISBOH-16 with 16 mol % hydroxyl groups, and the (ISBOH-24)/Cloisite 30B nanocomposite has ISBOH-24 with 24 mol % hydroxyl groups.

Figure 5 gives TEM images of (ISBOH-24)/Cloisite 15A, (ISBOH-24)/Cloisite 30B, and (ISBOH-39)/Cloisite 30B nanocomposites, showing that Cloisite 30B aggregates have a very high degree of dispersion in ISBOH-24, but a very low degree of dispersion in ISBOH-39, and Cloisite 15A aggregates also have a very low degree of dispersion in ISBOH-24. The observations made from the TEM images given in Figure 5 are consistent with those made from the XRD patterns given in Figure 4.

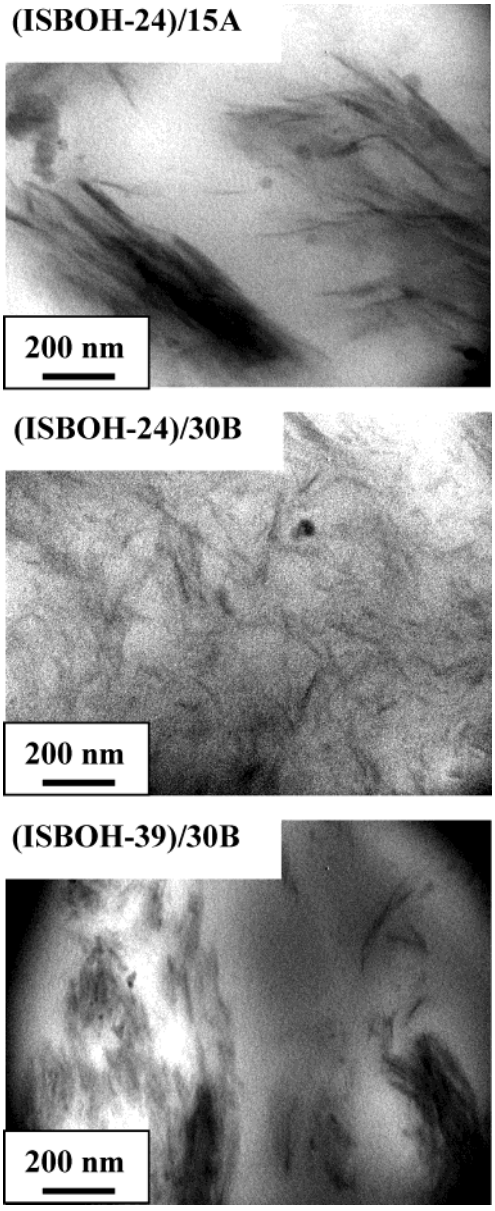

Figure 5. TEM images of (ISBOH-24)/Cloisite 15A nanocomposite, (ISBOH-24)/Cloisite 30B nanocomposite, and (ISBOH-39)/Cloisite 30B nanocomposite, in which the dark areas represent the clay and the gray/white areas represent the polymer matrix.

3.3. Temperature Dependence of Dynamic Storage Modulus for Organoclay Nanocomposites Based on SIS and SIOHS Triblock Copolymers. Figure 6 describes the temperature dependence of dynamic storage modulus (G') for a neat SIS triblock copolymer (○), SIS/Cloisite 30B nanocomposite (△), and SIS/Cloisite 15A nanocomposite (□), which were obtained from isochronal dynamic temperature sweep experiments at $\omega = 0.1$ rad/s. Note the neat SIS triblock copolymer has a 0.51 weight fraction of PS block (see Table 1), and thus it is expected to have lamellar microdomains below a certain critical temperature. In Figure 6, we observe that values of G' for the neat SIS triblock copolymer begin to drop precipitously at ca. 188 °C. Applying the empirical rheological criterion, which was first suggested by Guinlock and Porter in 1977,[26] we determined the order−disorder transition (ODT) temperature (T_{ODT}) of the SIS triblock copolymer to be ca. 188 °C. What is most interesting in Figure 6 is that both SIS/Cloisite 30B and SIS/Cloisite 15A nanocomposites have essentially the same T_{ODT} as the neat SIS triblock copolymer. This observation suggests that the addition of the organoclay, Cloisite 30B or Cloisite 15A, has affected *little,* if any, the ODT of the SIS triblock copolymer, signifying that little or no attractive interactions took place between the organoclay (Cloisite 30B or Cloisite 15A) and the SIS triblock copolymer. This observation supports the conclusion drawn above from the XRD patterns (see Figure 2).

Figure 7 describes the temperature dependence of G' for a hydroxylated neat triblock copolymer SIOHS-16 (○), (SIOHS-16)/Cloisite 30B nanocomposite (△), and (SIOHS-16)/Cloisite 15A nanocomposite (□), which were obtained from isochronal dynamic temperature sweep experiments at $\omega = 0.1$ rad/s. It is seen in Figure 7 that SIOHS-16 has a T_{ODT} of ca. 178 °C, which is about 10 °C lower than the T_{ODT} of the unfunctionalized precursor. This observation stands in contrast with the observation made in a previous study of Lee and Han,[20] who observed that the T_{ODT} of an SIOH diblock copolymer was higher than that of the unfunctionalized precursor. It is clear from Figure 7 that the addition of organoclay (Cloisite 30B or Cloisite 15A) has not affected the T_{ODT} of the neat block copolymer SIOHS-16, indicating that little or no attractive interactions took place

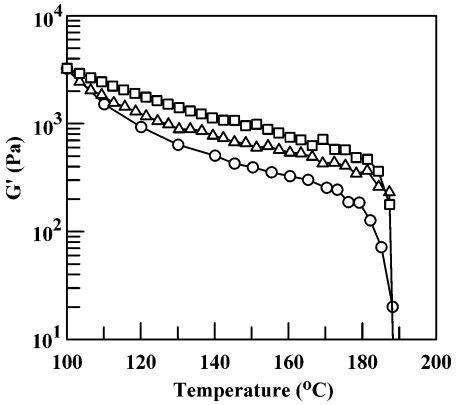

Figure 6. Variations of G' with temperature during isochronal dynamic temperature sweep experiments at $\omega = 0.1$ rad/s: (○) SIS triblock copolymer; (△) SIS/Cloisite 30B nanocomposite; (□) SIS/Cloisite 15A nanocomposite.

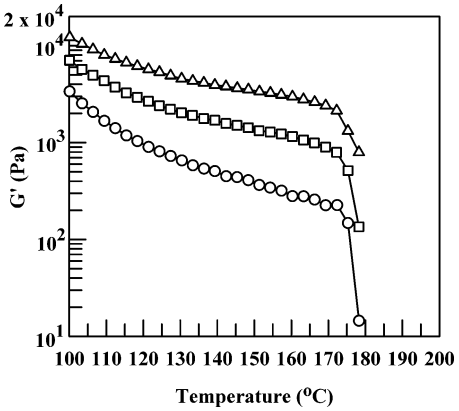

Figure 7. Variations of G' with temperature during isochronal dynamic temperature sweep experiments at $\omega = 0.1$ rad/s for: (○) triblock copolymer SIOHS-16; (△) (SIOHS-16)/Cloisite 30B nanocomposite; (□) (SIOHS-16)/Cloisite 15A nanocomposite.

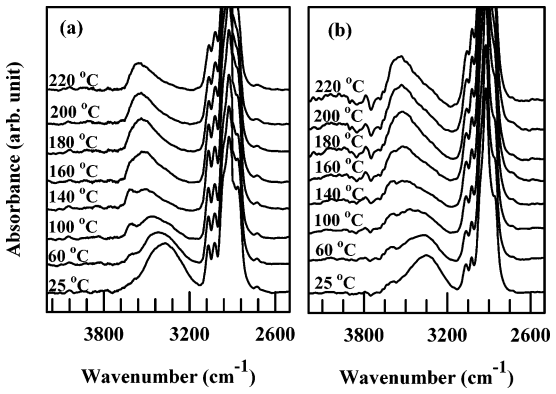

Figure 8. In situ FTIR spectra at various temperatures: (a) SIOHS-16 and (b) (SIOHS-16)/Cloisite 30B nanocomposite.

between the organoclay and SIOHS-16. This observation is consistent with that made above from the XRD patterns (see Figure 2) and TEM images (see Figure 3).

Figure 8 compares the FTIR spectra for the neat triblock copolymer SIOHS-16 with the FTIR spectra for the (SIOHS-16)/Cloisite 30B nanocomposite at temperatures ranging from 25 to 220 °C. Note that in FTIR spectroscopy the hydrogen-bonded and free hydroxyl groups appear at ca. 3330 and ca. 3630 cm^{-1}, respectively.[27] In Figure 8 we observe a remarkable similarity in FTIR spectra between the neat block copolymer

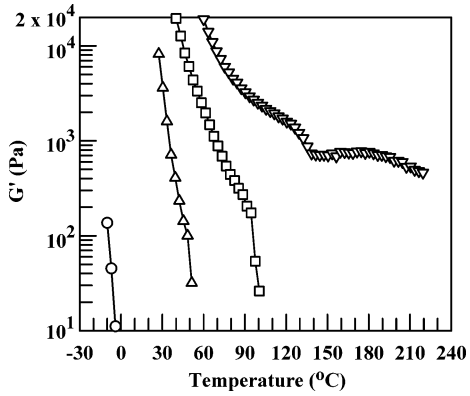

Figure 9. Variations of G' with temperature during isochronal dynamic temperature sweep experiments at $\omega = 0.1$ rad/s for triblock copolymers: (○) ISB; (△) ISBOH-16; (□) ISBOH-24; (▽) ISBOH-39.

SIOHS-16 and (SIOHS-16)/Cloisite 30B nanocomposite over the entire range of temperatures tested. Namely, the absorption band at ca. 3330 cm^{-1} persists up to ca. 60 °C and then begins to shift to a higher wavenumber at a temperature starting ca. 100 °C. This observation suggests that the hydrogen bonds that existed within the SIOHS-16 molecules disappeared as the temperature was increased above 60 °C and that little or no hydrogen bonds existed between the hydroxyl groups in the surfactant MT2EtOH residing at the surface of Cloisite 30B and the hydroxyl group in the midblock of SIOHS-16.

3.4. Temperature Dependence of Dynamic Storage Modulus for ISBOH Triblock Copolymers. Figure 9 describes the effect of the degree of hydroxylation of ISB triblock copolymer on the temperature dependence of G' during isochronal dynamic temperature sweep experiments at $\omega = 0.1$ rad/s: ISBOH-16 (△), ISBOH-24 (□), and ISBOH-39 (▽). For comparison, also given in Figure 9 is the temperature dependence of unfunctionalized precursor ISB (○). It is seen in Figure 9 that ISB is a homogeneous block copolymer, because values of G' decrease steadily with increasing temperature as in flexible ordinary homopolymers. This observation makes sense, because the molecular weight of ISB is very low, only 9.6×10^3 (see Table 1). Referring to Figure 9, values of G' for ISBOH-16 increased considerably, as compared to the unfunctionalized precursor, when the homogeneous ISB was hydroxylated yielding 16 mol % hydroxyl group. This amount of hydroxyl group in ISBOH-16 corresponds to ca. 40% hydroxylation of PB block with 1,2-addition in the ISB triblock copolymer (i.e., ISBOH-16 is a partially hydroxylated ISBOH triblock copolymer). In Figure 9 there is not a distinct temperature at which the value of G' drops abruptly, indicating that 40% hydroxylation of PB block with 1,2-addition in the ISB triblock copolymer is not sufficiently high to induce ODT in ISBOH-16. However, the values of G' in Figure 9 for ISBOH-24 increased considerably more as the amount of hydroxyl group was increased from 16 to 24 mol %, which correspond to ca. 60% hydroxylation of PB block with 1,2-addition in the ISB triblock copolymer (i.e., ISBOH-24 is a partially hydroxylated ISBOH triblock copolymer). In Figure 9, we observe very clearly that the values of G' for ISBOH-24 begin to drop very rapidly at ca. 100 °C, which can be assigned the T_{ODT} of ISBOH-24. Values of G' in Figure 9 for ISBOH-39 increased much further as the amount of hydroxyl group was

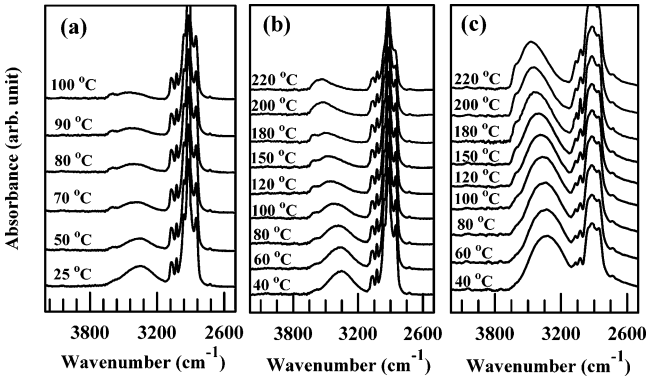

Figure 10. In situ FTIR spectra at various temperatures for triblock copolymers: (a) ISBOH-16; (b) ISBOH-24; (c) ISBOH-39.

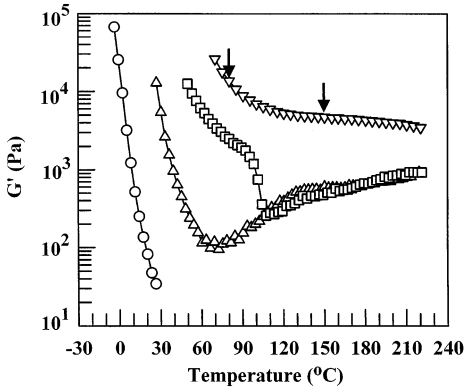

Figure 11. Variations of G' with temperature during isochronal dynamic temperature sweep experiments at $\omega = 0.1$ rad/s for nanocomposites: (○) ISB/Cloisite 30B; (△) (ISBOH-16)/Cloisite 30B; (□) (ISBOH-24)/Cloisite 30B; (▽) (ISBOH-39)/Cloisite 30B.

increased from 24 to 39 mol %, which corresponds to 100% hydroxylation of PB block with 1,2-addition in the ISB triblock copolymer (i.e., ISBOH-39 is a fully hydroxylated ISBOH triblock copolymer on the basis of 1,2-PB in ISB triblock copolymer). The temperature dependence of G' for ISBOH-39 (▽) in Figure 9 deserves special attention. Values of G' initially decrease rather slowly with increasing temperature and then suddenly stop at ca. 140 °C. As the temperature is increased further, values of G' show an increasing trend, going through a mild maximum at ca. 180 °C, followed by a decreasing trend. The temperature dependence of G' for ISBOH-39 looks completely different from that for ISBOH-24.

There are two possibilities that might explain the temperature dependence of G' for ISBOH-39 displayed in Figure 9. One possibility is that ISBOH-39 might undergo ODT at about 120 °C, at which point it is expected to attain a completely disordered state. Under this situation, values of G′ for ISBOH-39 at $T > 120$ °C should be negligibly small, in the same way as for the disordered ISBOH-24 observed in Figure 9, if little or no hydrogen bonding exists within the disordered ISBOH-39 molecules. However, Figure 9 shows that large values of G' persist in the *disordered* ISBOH-39 at $T > 120$ °C. This then suggests to us that there should exist some forces that keep values of G' for the disordered ISBOH-39 very large at $T > 120$ °C. Another possibility is that ISBOH-39 might undergo order−order transition (OOT) at about 140 °C, and therefore, it does not disorder over the entire range of temperatures investigated (up to ca. 220 °C). The above issue can be resolved if we investigate the morphology of ISBOH-39 by taking TEM images at temperatures below and above 120 °C. We will address this issue after we present the temperature dependence of G' for the (ISBOH-39)/Cloisite 30B nanocomposite during isochronal dynamic temperature sweep experiments.

Figure 10 gives in situ FTIR spectra for ISBOH-16, ISBOH-24, and ISBOH-39 over a wide range of temperatures. In Figure 10a, we observe that the absorption band at ca. 3330 cm^{-1} for ISBOH-16 persists up to 50 °C and then the absorption band at ca. 3330 cm^{-1} begins to shift to a higher wavenumber as the temperature is increased further. Thus, we conclude that the hydroxyl groups within ISBOH-16 molecules form hydrogen bonds, and they disappear at temperatures higher than ca. 50 °C. It is well documented in the literature[27] that the strength of hydrogen bonds decreases with increasing temperature.

In the in situ FTIR spectra for ISBOH-24 given in Figure 10b we observe that the absorption band at ca. 3330 cm^{-1} persists up to 100 °C, which is very close to the T_{ODT} of ISBOH-24 (see Figure 9). Notice that the area under the absorption band at ca. 3330 cm^{-1} in Figure 10b for ISBOH-24 is much larger than that in Figure 10a for ISBOH-16. This observation is reasonable, because the amount of hydroxyl group in ISBOH-24 is greater than that in ISBOH-16. We can then conclude that a sufficiently high degree of hydroxylation in ISBOH-24 has induced, via hydrogen bonding, ODT from a homogeneous triblock copolymer ISB. This conclusion is consistent with that made in a previous study of Lee and Han,[24] who induced ODT by hydroxylation of a homogeneous SI diblock copolymer, yielding microphase-separated SIOH diblock copolymer.

In the in situ FTIR spectra for ISBOH-39 given in Figure 10c, we observe that the absorption band at ca. 3330 cm^{-1} persists up to ca. 120 °C and then begins to shift to a slightly higher wavenumber at a temperature somewhere between 120 and 150 °C. Notice in Figure 10c that the area under the absorption band at ca. 3330 cm^{-1} for ISBOH-39 is very large, as compared to the area under the absorption band at ca. 3330 cm^{-1} for ISBOH-24 (Figure 10b). Again, this observation is due to the much larger amounts of hydroxyl groups present in ISBOH-39 than in ISBOH-24. What is noteworthy in the FTIR spectra for ISBOH-39, displayed in Figure 10c, is that very large area of absorption band in the vicinity of 3330 cm^{-1} persists even at 220 °C. We conclude that the presence of such a large absorption band in the vicinity of 3330 cm^{-1} at temperatures up to 220 °C might be responsible for the large values of G' for ISBOH-39 at 140−220 °C observed in the log G' vs temperature plot given in Figure 9. In other words, we attribute the large values of G' in ISBOH-39 at $T >$ ca. 140 °C (T_{ODT}), observed in Figure 9, to the strong hydrogen bonds within ISBOH-39 molecules.

3.5 Temperature Dependence of Dynamic Storage Modulus for Organoclay Nanocomposites Based on ISB and ISBOH Triblock Copolymers. Figure 11 describes the temperature dependence of G' during isochronal dynamic temperature sweep experiments at $\omega = 0.1$ rad/s for the following nanocomposites: ISB/Cloisite 30B (○), (ISBOH-16)/Cloisite 30B (△), (ISBOH-24)/Cloisite 30B (□), and (ISBOH-39)/Cloisite 30B (▽).

The following observations are worth noting in Figure 11. (i) Values of G' for ISB/Cloisite 30B nanocomposite (○) decrease steadily with increasing temperature as in ordinary flexible polymers. Such a temperature dependence of G' signifies that the addition of Cloisite 30B changed little the rheological behavior of neat ISB triblock copolymer. This observation suggests further that little attractive interactions exist between Cloisite 30B and ISB triblock copolymer. This observation is in good agreement with that made from XRD patterns (see Figure 4). After all, no functional group exists in the ISB triblock copolymer that can have attractive interactions with the hydroxyl groups in the surfactant MT2EtOH residing at the surface of Cloisite 30B. (ii) Values of G' for the (ISBOH-16)/Cloisite 30B nanocomposite (△) first decrease with increasing temperature until reaching ca. 60 °C, and then increase steadily with a further increase in temperature. (iii) Values of G' for the (ISBOH-24)/Cloisite 30B nanocomposite (□) first decrease slowly and then drop precipitously at ca. 100 °C followed by an increase with a further increase in temperature. (iv) Values of G' for the (ISBOH-39)/Cloisite 30B nanocomposite (▽) first decrease slowly with increasing temperature and then remain more or less constant with a further increase in temperature.

Comparison of Figure 11 with Figure 9 reveals that during isochronal dynamic temperature sweep experiments, the temperature dependence of G' for ISBOH-containing nanocomposites is quite different from that for neat ISBOH triblock copolymers. Specifically, (i) values of G' for the (ISBOH-16)/Cloisite 30B nanocomposite go through a minimum at ca. 70 °C as determined from Figure 11, whereas values of G' for ISBOH-16 decrease rapidly with increasing temperature as determined from Figure 9. (ii) Values of G' for the (ISBOH-24)/Cloisite 30B nanocomposite go through a minimum at ca. 110 °C as determined from Figure 11, whereas values of G' for ISBOH-24 begin to drop precipitously at about 100 °C as determined from Figure 9. (iii) Values of G' for both (ISBOH-39)/Cloisite 30B nanocomposite (Figure 11) and neat ISBOH-39 (Figure 9) decrease gradually with increasing temperature up to a certain critical value, and then remain more or less constant with a further increase in temperature. We now return to the question posed above as to whether a minimum in G' observed in Figure 11 represents ODT or OOT in ISBOH. To answer this question we obtained TEM images of (ISBOH-39)/Cloisite 30B nanocomposite samples, which were annealed for 30 min (i) at 80 °C followed by a rapid quenching into ice-cold water and (ii) at 150 °C followed by a rapid quenching into ice-cold water.

Figure 12 gives TEM images of the (ISBOH-39)/Cloisite 30B nanocomposite at (a) 80 and (b) 150 °C. It can be seen in Figure 12 that at 80 °C the (ISBOH-39)/Cloisite 30B nanocomposite has microdomains in the ISBOH-39 matrix, in which the organoclay nanoparticles are well dispersed. However, at 150 °C the microdomains in ISBOH-39 have disappeared completely, and only the organoclay nanoparticles are dispersed in the homogeneous matrix of ISBOH-39. The above TEM images lead us to conclude that (ISBOH-39)/Cloisite 30B nanocomposite undergoes ODT at a temperature somewhere between 80 and 150 °C. Although a precise determination of T_{ODT} for the (ISBOH-39)/Cloisite 30B nanocomposite from Figure 11 is difficult, we can estimate the T_{ODT} to be ca. 130 °C, at which values of G' begin to level off. We can then conclude further that the temperature at which G' goes through a minimum in Figure 11 signifies T_{ODT}; thus the T_{ODT} of (ISBOH-16)/Cloisite 30B nanocomposite is ca. 70 °C, and the T_{ODT} of (ISBOH-24)/Cloisite 30B nanocomposite is ca. 110 °C. Comparison of Figure 11 with Figure 9 reveals that the addition of Cloisite 30B to ISBOH-16 has induced microphase separation, which is attributable to the formation of hydrogen bonds between the hydroxyl groups in ISBOH-16 and the hydroxyl groups in the surfactant MT2EtOH residing at the surface of Cloisite 30B.

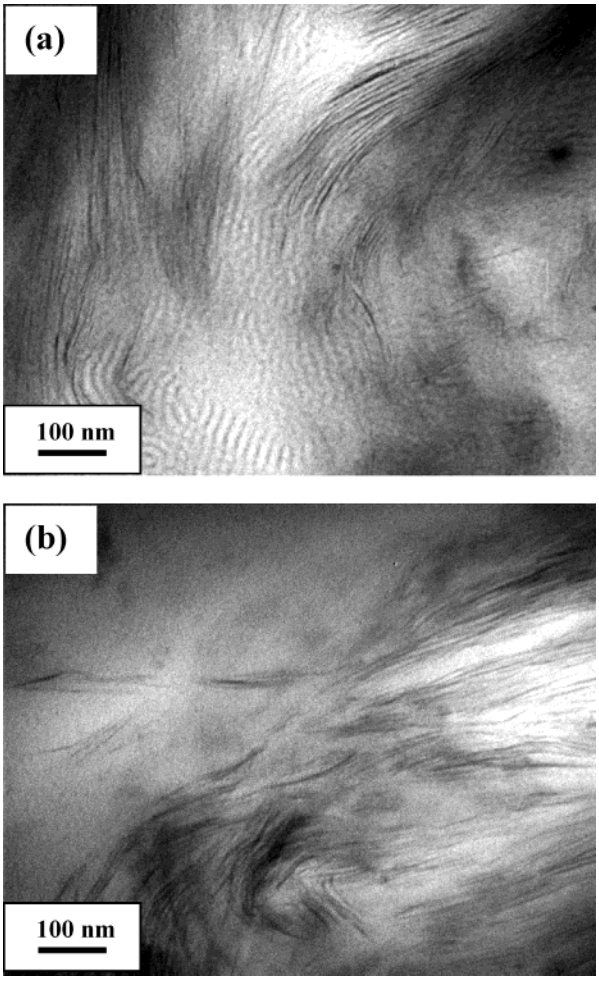

Figure 12. TEM images of (ISBOH-39)/Cloisite 30B nanocomposite (a) at 80 °C and (b) at 150 °C. Prior to taking TEM images, each specimen was annealed for 30 min at 80 °C or 150 °C followed by rapid quenching in ice-cold water.

Referring to Figure 11, a question yet to be answered is the following: Why do values of G' for the (ISBOH-39)/Cloisite 30B nanocomposite remain so large even after the disappearance of microdomains at $T > T_{ODT}$? Our answer to this question lies in the presence of strong hydrogen bonds between the hydroxyl groups in the surfactant MT2EtOH residing at the surface of Cloisite 30B and the hydroxyl groups in the ISBOH-39 matrix. Note that ISBOH-39 has very strong hydrogen bonds (see Figure 10). Figure 13 gives log G' vs log ω plots obtained from dynamic frequency sweep experiments at 200 °C for a neat SI diblock copolymer SI-14/3 (○) and hydroxylated SI diblock copolymer SI-14/3-OH (●). Figure 13 was prepared from the experimental data of Lee and Han,[28] who investigated the effect of hydroxylation of SI diblock on phase transition, and the

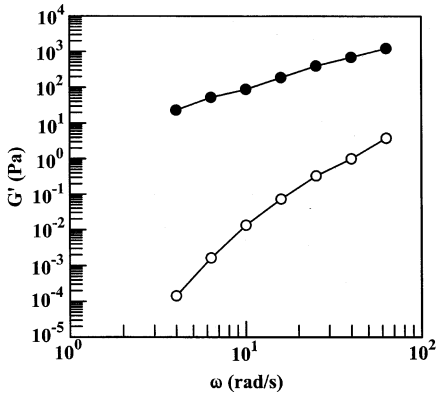

Figure 13. Plots of log G' vs log ω: (○) neat SI diblock copolymer SI-14/3 at 200 °C and (●) hydroxylated SI diblock copolymer SI-14/3-OH at 200 °C, showing that hydroxylation of SI-14/3 increased the values of G' 3−5 orders of magnitude depending upon the values of angular frequency ω applied.

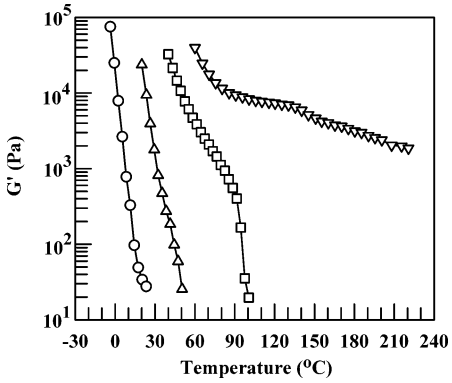

Figure 14. Variations of G' with temperature during isochronal dynamic temperature sweep experiments at $\omega = 0.1$ rad/s for nanocomposites: (○) ISB/Cloisite 15A; (△) (ISBOH-16)/Cloisite 15A; (□) (ISBOH-24)/Cloisite 15A; (▽) (ISBOH-39)/Cloisite 15A.

linear dynamic viscoelasticity of SI-14/3-OH. It can be seen in Figure 13 that values of G' for SI-14/3-OH are 3−5 orders of magnitude greater, depending on the angular frequency ω applied, than those for SI-14/3. This is attributable to the presence of hydrogen bonds within SI-14/3-OH molecules. Comparison of the data (▽) at $T > 140$ °C in Figure 11 with the data (▽) $T > 140$ °C in Figure 9 reveals further that values of G' for the (ISBOH-39)/Cloisite 30B nanocomposite are several times greater than those for the neat triblock copolymer ISBOH-39. This is attributable to the presence of hydrogen bonds between the hydroxyl groups in the surfactant MT2EtOH residing at the surface of Cloisite 30B and the hydroxyl groups in the ISBOH-39 matrix.

Note that (ISBOH-39)/Cloisite 30B nanocomposite has a poor dispersion of Cloisite 30B aggregates (see Figure 5) which, we now believe, is due to the presence of too strong hydrogen bonds within ISBOH-39 molecules, prohibiting hydrogen bonding between the hydroxyl group in the surfactant MT2EtOH residing at the surface of Cloisite 30B and the hydroxyl group in ISBOH-39. On the basis of the experimental observations made above, we can conclude that there exists an optimum degree of hydroxylation in ISBOH triblock copolymer that results in the most efficient dispersion of organoclay aggregates in organoclay/ISBOH triblock copolymer nanocomposites.

We carried out repeated rheological experiments using the same (ISBOH-16)/Cloisite 30B and (ISBOH-24)/Cloisite 30B nanocomposite samples. The results are given in the Supporting Information. We found that none of the rheological signatures observed in Figure 11 were lost. Also, we carried out repeated rheological experiments for (ISBOH-39)/Cloisite 15A nanocomposites, prepared from both unwashed and washed organoclay. The results are given in the Supporting Information, indicating that the repeated measurements are reproducible and that the excess amount of surfactant (2M2HT) residing at the surface of Cloisite 15A appears to have played little or no role in the rheological behavior of the (ISBOH-39)/Cloisite 15A nanocomposite. Further, we prepared additional (ISBOH-16)/Cloisite 30B and (ISBOH-24)/Cloisite 30B nanocomposites by washing the organoclay with methanol and then carried out rheological measurements. The results are given in the Supporting Information. We obtained a reasonably good agreement with the results presented in Figure 11, indicating that little cross-linking reactions appear to have occurred between the organoclay and polymer matrix during the rheological measurements. We measured, via GPC, the molecular weight and molecular weight distribution of the polymer samples prior to and after the nanocomposites were exposed to high temperatures, in the presence of the layered silicates, during rheological measurements. For this, polymers were extracted by dissolving nanocomposites in a common solvent followed by filtration. The values of M_w and M_w/M_n thus determined and also the GPC traces for the polymer samples are given in the Supporting Information. We have concluded that the values M_w and M_w/M_n for the polymer samples prior to and after the rheological measurements remain virtually the same within experimental uncertainties associated with GPC measurements.

Figure 14 describes the temperature dependence of G' during isochronal dynamic temperature sweep experiments at $\omega = 0.1$ rad/s for the following nanocomposites: ISB/Cloisite 15A (○), (ISBOH-16)/Cloisite 15A (△), (ISBOH-24)/Cloisite 15A (□), and (ISBOH-39)/Cloisite 15A (▽). The following observations are worth noting in Figure 14. Comparison of Figure 14 with Figure 9 reveals that the addition of Cloisite 15A has changed *little* the temperature dependence of G' for ISB, ISBOH-16, ISBOH-24, or ISBOH-39, indicating that the presence of Cloisite 15A is of no consequence in the respective nanocomposites. However, values of G' for the (ISBOH-39)/Cloisite 15A nanocomposite (▽ in Figure 14) are larger than those of neat ISBOH-39 (▽ in Figure 9). This is attributable to the intercalation of organoclay Cloisite 15A by ISBOH-39 in the (ISBOH-39)/Cloisite 15A nanocomposite. Evidence of intercalation of Cloisite 15A in the (ISBOH-24)/Cloisite 15A nanocomposite, although the degree of intercalation is not high, can be seen in the TEM image given in Figure 5. This observation suggests that Cloisite 15A aggregates must have been dispersed poorly in all four nanocomposites: ISB/Cloisite 15A, (ISBOH-16)/Cloisite 15A, (ISBOH-24)/Cloisite 15A, and (ISBOH-39)/Cloisite 15A. This indeed turns out to be case as we already have observed from the XRD patterns (see Figure 4) and TEM image (see Figure 5). It is worth noting the dramatic difference in the temperature dependence of G' (i) between the (ISBOH-16)/Cloisite 15A nanocomposite (△ in Figure 14) and the (ISBOH-16)/Cloisite 30B nanocomposite (△ in Figure 11) and (ii) between the (ISBOH-24)/Cloisite 15A nanocomposite (□ in Figure 14) and the (ISBOH-24)/Cloisite 30B nanocomposite (□ in Figure 11). The origin

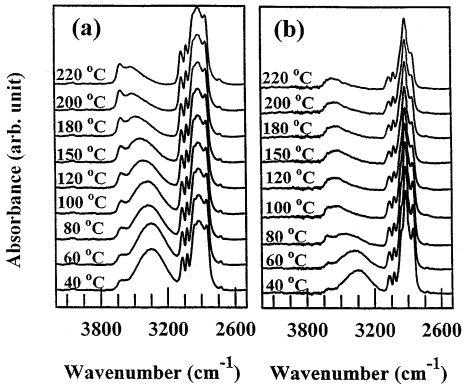

Figure 15. In situ FTIR spectra at various temperatures for: (a) (ISBOH-24)/Cloisite 30B nanocomposite and (b) (ISBOH-24)/Cloisite 15A nanocomposite.

of the differences between the two situations can be found from the FTIR spectra given in Figure 15.

Specifically, Figure 15a gives in situ FTIR spectra for the (ISBOH-24)/Cloisite 30B nanocomposite at various temperatures, and Figure 15b gives in situ FTIR spectra for the (ISBOH-24)/Cloisite 15A nanocomposite at various temperatures. Comparison of Figure 15a with Figure 10b reveals that the area under the absorption band at ca. 3330 cm^{-1} is larger in the (ISBOH-24)/Cloisite 30B nanocomposite than in neat ISHOH-24 at temperatures ranging from 60 to 150 °C. The much larger area under the absorption band at ca. 3330 cm^{-1} signifies the presence of the hydrogen bonds between the hydroxyl group in the surfactant MT2EtOH residing at the surface of Cloisite 30B and the hydroxyl group in ISBOH-24. That is, attractive interactions exist between Cloisite 30B and ISBOH-24 in (ISBOH-24)/Cloisite 30B nanocomposite. The presence of such attractive interactions, owing to hydrogen bonding, is responsible for the increasing trend of G' with increasing temperature above the T_{ODT} of ISBOH-24 observed in Figure 11. We wish to mention at this juncture that the in situ FTIR spectra presented in this paper are qualitative in nature and they are intended to identify the origin of the dispersion characteristics and rather unusual rheological behavior of the (ISBOH-16)/Cloisite 30B and (ISBOH-24)/Cloisite 30B nanocomposites. Quantitative analysis (e.g., the determination of the percentage of hydrogen bonding sites on the Cloisite 30B surface) of the in situ FTIR spectra by deconvoluting the overlapping peaks in the FTIR spectra shown in Figure 15, for example, has been found to be extremely difficult, since the amount of the hydroxyl groups associated with the organoclay Cloisite 30B in the nanocomposite was so small (estimated to be less than 0.2%). Moreover, quantitative analysis of FTIR spectra is beyond the scope of this paper.

In Figure 15b, we observe no evidence of the presence of hydrogen bonds between the surfactant 2M2HT residing at the surface of Cloisite 15A and the hydroxyl group in ISBOH-24. This observation is not surprising, because the surfactant 2M2HT residing at the surface of Cloisite 15A has no polar group that can have attractive interactions with the hydroxyl group in ISBOH-24. Under such circumstances, one cannot expect to have a high degree of dispersion of Cloisite 15A aggregates in ISBOH-24. This indeed turns out to be the case as we have already observed from the TEM image given in Figure 5. Comparison of parts a and b of Figure 15 reveals a dramatic difference in in situ

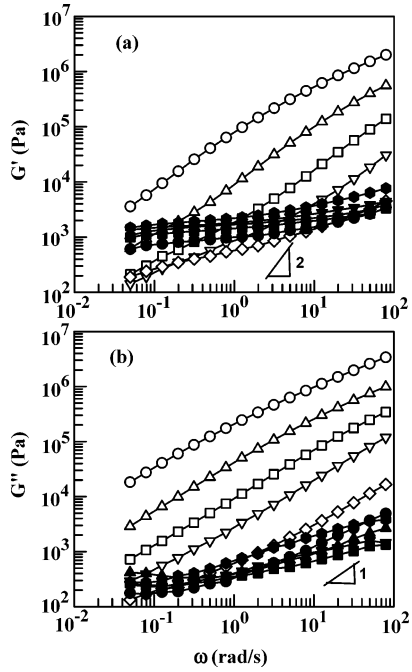

Figure 16. (a) The log G' vs log ω plots and (b) log G'' vs log ω plots for the (ISBOH-16)/Cloisite 30B nanocomposite at various temperatures: (○) 30, (△) 40, (□) 50, (▽) 60, (◊) 80, (●) 100, (▲) 120, (■) 160, (▼) 200, and (●) 220 °C.

FTIR spectra between the (ISBOH-24)/Cloisite 30B and (ISBOH-24)/Cloisite 15A nanocomposites. Such a dramatic difference in in situ FTIR spectra between the two nanocomposites explains why the (ISBOH-24)/Cloisite 30B nanocomposite has a very high degree of dispersion of Cloisite 30B aggregates in ISBOH-24, while the (ISBOH-24)/ Cloisite 15A nanocomposite has a very poor dispersion of Cloisite 15A aggregates in ISBOH-24 (see Figure 5).

3.6. Linear Dynamic Viscoelasticity of Nanocomposites Based on ISB and ISBOH Triblock Copolymers. Figure 16 gives log G' vs log ω and log G'' vs log ω plots for the (ISBOH-16)/Cloisite 30B nanocomposite at various temperatures ranging from 30 to 220 °C. In Figure 16a, we observe that the slope of log G' vs log ω plots begins to change at ca. 60 °C, and the (ISBOH-16)/Cloisite 30B nanocomposite exhibits solidlike behavior beginning at ca. 100 °C. The most unusual observation that can be made from the log G' vs log ω plots given in Figure 16a is that values of G' increase with increasing temperature beginning at ca. 100 °C. Somewhat similar observation can be made from the log G'' vs log ω plots given in Figure 16b.

Figure 17 gives log G' vs log G'' plots for the (ISBOH-16)/Cloisite 30B nanocomposite at various temperatures ranging from 30 to 140 °C. It has amply been demonstrated that the log G' vs log G'' plots for monodisperse flexible homopolymers are expected to be independent of temperature and to have a slope of 2 in the terminal region.[29−31] Such plots have successfully been used to determine the T_{ODT} of microphase-separated block copolymers.[32−34] The inset of Figure 17 gives the results of isochronal dynamic temperature sweep experiment at $\omega = 0.1$ rad/s. The most unusual observation that can be made from Figure 17 is that in the terminal region of log G' vs log G'' plots, values of G' begin to increase with increasing temperature beginning at ca. 60 °C. This temperature is close to the temperature at which values of G' begin to increase during the iso-

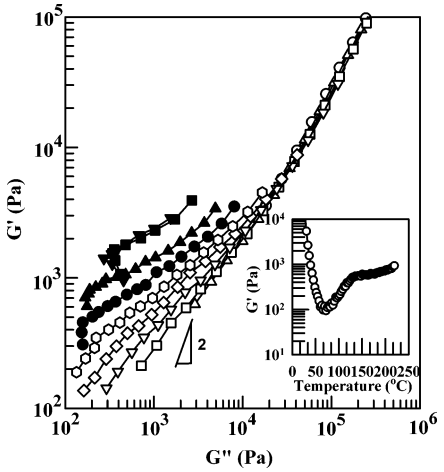

Figure 17. The log G' vs log G'' plots for the (ISBOH-16)/Cloisite 30B nanocomposite at various temperatures: (○) 30, (△) 40, (□) 50, (▽) 60, (◊) 70, (⬠) 80, (●) 90, (▲) 100, (■) 120, and (▼) 140 °C.

chronal dynamic temperature sweep experiment shown in the inset of Figure 17. In Figure 17, we observe that values of G' in log G' vs log G'' plots begin to increase with increasing temperature beginning at ca. 60 °C. Similar observations were also made, although not presented here, for the (ISBOH-24)/Cloisite 30B nanocomposite. Previously, Lee and Han[20] investigated linear dynamic viscoelasticity of nanocomposites composed of Cloisite 30B and an SIOH diblock copolymer and also made similar observations. They attributed the very unusual experimental observation, an increase in G' with increasing temperature in log G' vs log G'' plots, to the increase in surface area of the organoclay Cloisite 30B owing to an enhanced dispersion of Cloisite 30B aggregates.

At this juncture we wish to point out that under the circumstances where specific interactions exist in such organoclay nanocomposites as those investigated in this study, no attempt should be made to apply time–temperature superposition (TTS). This is quite obvious from Figure 16, since there is no way one can obtain temperature-independent reduced plots by shifting log G' vs log ω and log G'' vs log ω plots along the ω axis. Log G′ vs log G'' plots given in Figure 17, which were prepared from Figure 16, demonstrate very clearly that TTS would fail for such nanocomposites. It is well established that TTS fails, for instance, in miscible polymer blends forming hydrogen bonds via specific interactions. The readers are reminded that in Figure 15 we have shown FTIR spectra for the (ISBOH-24)/Cloisite 30B nanocomposite, demonstrating that intermolecular hydrogen bonds are formed between the hydroxyl groups in ISBOH-24 and the hydroxyl groups in the surfactant MT2EtOH residing at the surface of Cloisite 30B. The FTIR spectra for the (ISBOH-16)/Cloisite 30B nanocomposite also show the formation of intermolecular hydrogen bonds between the hydroxyl groups in ISBOH-16 and the hydroxyl groups in the surfactant MT2EtOH residing at the surface of Cloisite 30B although they are not presented here owing to the space limitations.

3.7. Effect of Triblock Copolymer Architecture on the Dispersion Characteristics of Organoclay in Nanocomposites. We would like to address the issue as to why Cloisite 30B aggregates have a poor dispersion in SIOHS/Cloisite 30B nanocomposite, while the same organoclay aggregates have a very good dispersion in (ISBOH-16)/Cloisite 30B or (ISBOH-24)/Cloisite 30B nanocomposites (compare Figure 3 with Figure 5). According to Turner,[35] a microphase-separated lamella-forming ABA-type triblock copolymer can adopt one of two conformations: either it can "bridge" two exterior A-regions or it can form a "loop" where both its A-blocks lie in the same region (see Figure 1 of ref 35). The SIS triblock copolymer employed in the present study has a 0.46 weight fraction of PS block (see Table 1), thus forming lamellar microdomains. Note that the hydroxyl groups in the PIOH chain of an SIOHS triblock copolymer are located in the middle, flanked by two long PS end blocks. Under such circumstances, the hydroxyl groups in the PIOH midblock of an SIOHS triblock copolymer might form strong hydrogen bonds within SIOHS molecules and thus would have much *fewer* chances to form hydrogen bonds with the hydroxyl groups in the surfactant MT2EtOH residing at the surface of Cloisite 30B, especially when two PS end blocks in an SIOHS chain form "loops" rather than "bridges."

Further, exfoliation of organoclay aggregates requires that the polymer molecules approach the surface of the layered silicates and then peel away the top and bottom layers as promoted by polymer adsorption and the application of shear stress. In this regard, ISBOH molecules have an advantage over SIOHS molecules, because the PBOH molecules are located at one end of an ISBOH chain, which can then easily approach the surface of Cloisite 30B and then form hydrogen bonds with the hydroxyl groups in the surfactant MT2EtOH. On the other hand, the hydroxylated PIOH molecules in an SIOHS triblock copolymer are located in the middle, while two chemically very inert PS blocks are located at both ends of an SIOHS chain. It would be very difficult for the PIOH midblock of an SIOHS chain to approach the hydroxyl group in the surfactant MT2EtOH residing at the surface of the Cloisite 30B and then peel away the top and bottom layers, while two PS end blocks of the same SIOHS chain are repulsive to the surfactant MT2EtOH. In other words, in the *absence* of attractive interactions between the PS molecules at the end of SIOHS chain and the surfactant MT2EtOH residing at the surface of Cloisite 30B, the diffusion of PS end blocks into the galleries of layered Cloisite 30B would be very difficult if not very unlikely. This observation now explain why very poor dispersion of Cloisite 30B aggregates is observed in the (SIOHS-16)/Cloisite 30B nanocomposite (see Figure 3).

It happens that in the present study we employed an SIS triblock copolymer and hydroxylated it to obtain SIOHS triblock copolymer, while we employed an ISB triblock copolymer and hydroxylated it to obtain ISBOH triblock copolymer. We expect that the conclusions drawn from the use of an SIOHS triblock copolymer in the present study would be the same even if we had used a hydroxylated SBOHS triblock copolymer. This expectation is based on the notion that chain ends are important for adsorption. That is, both SBOHS and SIOHS triblock copolymers would not be effective in dispersing the aggregates of organoclay Cloisite 30B as long as the hydroxylated block, PBOH or PIOH, resides in the middle of an ABA-type triblock copolymer.

In this study we have shown that the presence of a functionalized block at chain ends is effective to obtain

a high degree of exfoliation in organoclay nanocomposites based on functionalized triblock copolymers.

4. Concluding Remarks

The experimental results presented in this paper show unequivocally that the ISBOH triblock copolymers with an optimum amount of hydroxyl group are tremendously more effective than the SIOHS triblock copolymer in achieving a very high degree of dispersion (exfoliation) of Cloisite 30B aggregates (compare Figure 5 with Figure 3). This was made possible owing to the presence of attractive interactions between the hydroxyl group in ISBOH triblock copolymer and the hydroxyl group in the surfactant MT2EtOH residing at the surface of Cloisite 30B. We have also shown that the same ISBOH triblock copolymers are totally ineffective to achieve a very high degree of exfoliation of Cloisite 15A aggregates (see Figure 5), owing to a lack (or absence) of attractive interactions between the ISBOH block copolymer and the surfactant 2M2HT residing at the surface of Cloisite 15A. This experimental observation points out the utmost importance (or necessity) of attractive interactions between a polymer matrix and an organoclay in order to achieve a high degree of exfoliation of organoclay aggregates in nanocomposites. The present study indicates that, even in the presence of attractive interactions between a polymer matrix and an organoclay, the architecture of triblock copolymers has a profound influence on the dispersion characteristics of Cloisite 30B aggregates. On the other hand, Cloisite 15A aggregates had a low degree of dispersion in both ISBOH and SIOHS triblock copolymers. We also have shown that there exists an optimum degree of hydroxylation in an ISBOH triblock copolymer in that too high a degree of hydroxylation in an ISBOH triblock copolymer forms too strong hydrogen bonding, prohibiting hydrogen bonding between the polymer matrix and the surfactant residing at the surface of Cloisite 30B in a given ISBOH/Cloisite 30B nanocomposite.

In this paper, using in situ FTIR spectroscopy, we have presented clear evidence that hydrogen bonds were formed between the hydroxyl groups in ISBOH and the hydroxyl groups in the surfactant MT2EtOH residing at the surface of Cloisite 30B, but *not* between the hydroxyl groups in SIOHS and the hydroxyl groups in the surfactant MT2EtOH residing at the surface of Cloisite 30B. We have explained the differences observed between the ISBOH/Cloisite 30B and SIOHS/Cloisite 30B nanocomposites in terms of the locations of the hydroxyl groups in the respective triblock copolymers.

In the present study, we also investigated the dispersion characteristics of two additional nanocomposites (with 5 wt % Cloisite 30B) using commercial ABA-type triblock copolymers: (i) an SIS triblock copolymer (Vector 4111, Dexco Polymers Company) having a 0.183 weight fraction of PS block and $M_w = 1.4 \times 10^5$, and (ii) a polystyrene-*block*-poly(ethylene-*co*-1-butene)-*block*-polystyrene (SEBS triblock) copolymer with maleic anhydride (MA) grafted onto the poly(ethylene-*co*-1-butene) (PEB) midblock, SEBS-*g*-MA (FG-1901X, Kraton Products Company), having a 0.3 weight fraction of PS block, $M_w = 5.6 \times 10^4$, and 1.7 wt % MA grafted. SEBS-*g*-MA was chosen, because the carbonyl group in maleic anhydride, which was grafted onto the PEB midblock of an SEBS triblock copolymer, can *potentially* have attractive interactions, via hydrogen bonding, with the hydroxyl group in the surfactant MT2EtOH residing at the surface of Cloisite 30B. The results of our TEM study, although not presented here, show that Cloisite 30B aggregates have very poor dispersion in both Vector 4111/Cloisite 30B and (SEBS-*g*-MA)/Cloisite 30B nanocomposites. Such an observation is not surprising because, on the basis of the experimental results presented in Figures 3 and 4, little or no attractive interactions can be expected between the surfactant MT2EtOH residing at the surface of Cloisite 30B and Vector 4111 and between the surfactant MT2EtOH residing at the surface of Cloisite 30B and SEBS-*g*-MA.

We conclude that the experimental results presented in this paper shed light on the future direction of designing triblock copolymers for the preparation of organoclay nanocomposites having a very high degree of exfoliation.

Acknowledgment. We acknowledge with gratitude that Southern Clay Products Inc. provided us with the organoclays employed in this study. This study was supported in part by LG Chemical Ltd.

Supporting Information Available: A table of molecular characteristics of SIOHS and ISBOH and figures showing IR spectra of Cloisite 30B, GPC data, and G' vs temperature data. This material is available free of charge via the Internet at http://pubs.acs.org.

References and Notes

(1) (a) Usuki, A.; Kawasumi, M.; Kojima, Y.; Okada, A.; Kurauchi, T.; Kamigaito, O. *J. Mater. Res.* **1993**, *8*, 1174. (b) Kojima, Y.; Usuki, A.; Kawasumi, M.; Okada, A.; Kurauchi, T.; Kamigaito, O. *J. Polym. Sci., Polym. Chem. Ed.* **1993**, *31*, 983. (c) Yano, K.; Usuki, A.; Okada, A.; Kurauchi, T.; Kamigaito, O. *J. Polym. Sci., Polym. Chem. Ed.* **1993**, *31*, 2493. (d) Kojima, Y.; Usuki, A.; Kawasumi, M.; Okada, A.; Kurauchi, T.; Kamigaito, O.; Kaji, K. *J. Polym. Sci., Polym. Phys. Ed.* **1994**, *32*, 625. (e) Kojima, Y.; Usuki, A.; Kawasumi, M.; Okada, A.; Kurauchi, T.; Kamigaito, O.; Kaji, K. *J. Polym. Sci., Polym. Phys. Ed.* **1995**, *33*, 1039.

(2) Messersmith, P. B.; Giannelis, E. P. *Chem. Mater.* **1993**, *5*, 1064. Messersmith, P. B.; Giannelis, E. P. *J. Polym. Sci., Polym. Phys. Ed.* **1995**, *33*, 1047.

(3) Krishnamoorti, R.; Giannelis, E. P. *Macromolecules* **1997**, *30*, 4097.

(4) Hoffmann, B.; Kressler, J.; Stöppelmann, G.; Fredrich, C.; Kim, G.-M. *Colloid Polym. Sci.* **2000**, *278*, 629.

(5) Lepoittevin, B.; Pantoustier, N.; Devalckenaere, M.; Alexandre, M.; Kubies, D.; Calberg, D.; Jérôme, R.; Dubois, P. *Macromolecules* **2002**, *35*, 8385.

(6) Vaia, R. A.; Giannelis, E. P. *Macromolecules* **1997**, *30*, 7990.

(7) Vaia, R. A.; Giannelis, E. P. *Macromolecules* **1997**, *30*, 8000.

(8) Balazs, A. C.; Singh, C.; Zhulina, E. *Macromolecules* **1998**, *31*, 8370.

(9) Zhulina, E.; Singh, C.; Balazs, A. C. *Langmuir* **1999**, *15*, 3935.

(10) Lee, K. M.; Han, C. D. *Polymer* **2003**, *44*, 4573 and references therein.

(11) Lee, K. M.; Han, C. D. *Macromolecules* **2003**, *36*, 7165 and references therein.

(12) Burke, J. J.; Weiss, V. Eds.; *Block and Graft Copolymers*, Syracuse University Press: Syracuse, NY, 1973.

(13) Noshay, A.; McGrath, J. E. *Block Copolymers*; Academic Press: New York, 1977.

(14) Hamley, I. W. *The Physics of Block Copolymers*, Oxford University Press: Oxford, England, 1998.

(15) Ren, J.; Silva, A. S.; Krishnamoorti, R. *Macromolecules* **2000**, *33*, 3739.

(16) Ren, J.; Krishnamoorti, R. *Macromolecules* **2003**, *36*, 4443.

(17) Mitchell, C. A.; Krishnamoorti, R. *J. Polym. Sci., Polym. Phys. Ed.* **2002**, *40*, 1434.

(18) Krishnamoorti, R.; Silva, A. S.; Mitchell, C. A. *J. Chem. Phys.* **2001**, *115*, 7175.

(19) Silva, A. S.; Mitchell, C. A.; Tse, M. F.; Wang, H.-C.; Krishnamoorti, R. *J. Chem. Phys.* **2001**, *115*, 7166.

(20) Lee, K. M.; Han, C. D. *Macromolecules* **2003**, *36*, 804.

(21) Halasa, A. F.; Lohr, D. F.; Hall, J. E. *J. Polym. Sci., Polym. Chem. Ed.* **1981**, *19*, 1357.
(22) Brown, H. C. *Hydroboration*; Benjamin: New York, 1962.
(23) Chung, T. C.; Raate, M.; Berluche, E.; Schulz, D. N. *Macromolecules* **1988**, *21*, 1903.
(24) Lee, K. M.; Han, C. D. *Macromolecules* **2002**, *35*, 760.
(25) Physical Properties Bulletin from Southern Clay Products, Inc.
(26) Gouinlock, E. V.; Porter, R. S. *Polym. Eng. Sci.* **1977**, *17*, 535.
(27) Coleman, M. M.; Graf, J. F.; Painter, P. C. *Specific Interactions and the Miscibility of Polymer Blends*, Technomic: Lancaster, PA, 1991.
(28) Lee, K. M.; Han, C. D. *Macromolecules* **2002**, *35*, 760. SI-14/3 is a homogeneous block copolymer having $M_n = 1.7 \times 10^4$, $M_w/M_n = 1.08$, and a 0.84 fraction of PS block. The hydroxylation of SI-14/3 induced microphase separation, yielding a cylinder-forming SI-14/3-OH having a T_{ODT} of ca. 195 °C. Thus, to compare the linear dynamic viscoelasticity data for SI-14/3-OH in the disordered state at 200 °C (Figure 13 in ref 28) with the linear dynamic viscoelasticity data for SI-14/3, we had to extrapolate the data for SI-14/3 that are available only at temperatures ranging from 95 to 125 °C (Figure 10, ref 28). Due to such a low molecular weight of SI-14/3, it would not have been possible for Lee and Han to have obtained linear dynamic viscoelasticity data for SI-14/3 at temperatures as high as 200 °C.
(29) Han, C. D.; Jhon, M. S. *J. Appl. Polym. Sci.* **1986**, *32*, 3809.
(30) Han, C. D.; Kim, J. K. *Macromolecules* **1989**, *22*, 4292.
(31) Han, C. D. *J. Appl. Polym. Sci.* **1988**, *35*, 167.
(32) Han, C. D.; Kim, J. *J. Polym. Sci., Polym. Phys. Ed.* **1987**, *25*, 1741.
(33) Han, C. D.; Kim, J.; Kim, J. K. *Macromolecules* **1989**, *22*, 383.
(34) Han, C. D.; Baek, D. M.; Kim, J. K. *Macromolecules* **1990**, *23*, 561.
(35) Turner, M. S. M*acromolecules* **1995**, *28*, 6878.

MA030585S